Theoretical and Applied Fracture Mechanics 135 (2025) 104772

Contents lists available at ScienceDirect

Theoretical and Applied Fracture Mechanics

journal homepage: www.elsevier.com/locate/tafmec

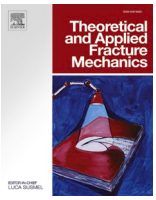

Fatigue characterisation of structural steel by means of the small punch test: Development of a methodology

S. Otero *, G. Álvarez, M.M. Llera, C. Rodríguez

SIMUMECAMAT Research Group. University of Oviedo, West Building. 7.1.10. University Campus, 33203 Gijón, Asturias, Spain

ARTICLE INFO

Keywords:
SPT-fatigue test
Rotating beam fatigue test
S-N curve
S_{PT}-N *iso*-damage curves
K_{SPT}

ABSTRACT

Knowledge of the fatigue behaviour of materials is fundamental to the safe design of structures. Standardised tests are used for this purpose, but their application requires a considerable amount of material, which in many cases is not available. To overcome this problem, the use of miniature tests would be the optimal solution. This work analyses the application of the Small Punch Test (SPT) to characterise the fatigue behaviour of structural steels. To this end, an experimental methodology has been developed to analyse not only where SPT-fatigue damage initiates and how it propagates, but also its relationship with changes in specimen compliance. Based on this methodology, different S_{PT}-N *iso*-damage curves and the SPT-fatigue limit have been obtained for two structural steels. By comparing these results with those obtained from rotating beam fatigue tests, a simple correlation has been proposed between the fatigue limits obtained from SPT and rotating beam fatigue tests.

1. Introduction

Understanding of the fatigue behaviour of the individual mechanical components of a large structure is essential to ensure structural integrity under varying loads [1,2]. For this purpose, there are well-defined test procedures based on well-known and established standards [3,4] which specify the geometry and size of the test specimens, usually of considerable volume. These test procedures cannot be used when the amount of material available is insufficient or the element from which the specimens are to be extracted must remain in service. In such cases, alternative tests such as hardness or miniature testing can be used [5–7]. However, the results, although related to fatigue, are often closely tied to microstructural factors, occasionally leading to inaccurate predictions [8,9]. For this reason, tests such as the Small Punch Test (SPT), which uses much smaller specimens while providing appropriate mechanical parameters, are indicated [10–15]. The Small Punch Test (SPT), initially proposed by Manahan et al. at MIT, was developed to characterise post-irradiation materials in nuclear power plants [16]. Currently, the most common applications of the SPT remain tensile and creep tests [17]. This test is simple and economical, and it can estimate key tensile parameters, such as yield strength and ultimate tensile strength, using small square or circular specimens (10x10mm or 10 mm diameter, respectively) and a thickness of only 0.5 mm. The effectiveness of the SPT in obtaining tensile parameters under quasi-static test conditions makes it one of the most widely used miniature tests, particularly for metallic materials [15,18–23]. So much so that in 2022, the CEN issued the first European Standard regulating the procedure and proper execution of the SPT, the parameters which it can obtain, and the correlations between these parameters and tensile mechanical properties [24,25].

Fig. 1.a) illustrates the most common configuration of the test: the contour of the specimen is embedded between two dies and subsequently deformed under the action of a semi-spherical punch with a diameter of 2.5 mm, passing through a 4 mm diameter die. During the test, the values of applied load and punch displacement are recorded, yielding the characteristic curve of the test, (Fig. 1.b). This curve defines various regions and characteristic points from which tensile mechanical properties are derived.

The curve shown in Fig. 1.b) is divided into 4 regions, indicated at the top of the graph. Zone I corresponds to the elastic bending of the sample. Zone II represents the onset of plastic deformation. In Zone III, plastic bending leads to membrane behaviour. In Zone IV, failure micromechanisms develop (necking and internal cracking) until specimen failure occurs. In the transition zone between Zone I and Zone II, the yield load, P_y is defined. This load is directly related to the yield stress of the material with expressions like (1), where t is the initial thickness of the specimen. It is also possible to obtain the ultimate tensile strength, σ_{ut}, from the SPT values of load (P_m) and displacement (d_m) at maximum, using expression (2) [11].

* Corresponding author.
E-mail address: oterosara@uniovi.es (S. Otero).

https://doi.org/10.1016/j.tafmec.2024.104772
Received 11 June 2024; Received in revised form 19 November 2024; Accepted 19 November 2024
Available online 24 November 2024

$$\sigma_{ys} = \alpha \cdot \frac{P_y}{t^2} \quad (1)$$

$$\sigma_{ut} = \beta \cdot \frac{P_m}{t \cdot d_m} \quad (2)$$

Being α and β constants whose values are well defined in the literature [10–14] and in the standard [24].

Once the good correlation between SPT and tensile parameters under quasi-static loading has been demonstrated, it would be convenient to explore its applicability under fatigue loading, attempting to establish a correlation between the behaviour of steels obtained by standard fatigue procedures (such as rotating beam fatigue test) and those obtained using the SPT.

To date, there has been little research into a methodology to characterize fatigue using miniature tests [26–31]. Most of it has been carried out at the Indian Institute of Technology, where the ball indentation method (ABI) developed by Prakash et al. [32] was adapted to characterize the mechanical behaviour of different materials under fatigue loads [33]. As far as the SPT is concerned, R.J. Lancaster et al. [34] used the SPT in fatigue behavior analysis of Ti-6Al-4 V alloy. They developed a dual-punch system, with one punch located at the top and the other at the bottom of the specimen, which subjected it to alternating load (R = -1). However, this study [34] did not develop a specific testing methodology, but merely applied alternating loads, well above the yield load, P_y, (which do not correspond to the loads used in conventional S-N tests), recording the number of cycles to failure. Subsequently, the same research group, [35], used the SPT again to analyse the fatigue behavior of a nickel-based superalloy, C263, obtained by additive manufacturing. On this occasion, a standard SPT device (single punch) and a load ratio of R = 0.1 were used, although again using loads well above the yield load, P_y, of the material.

The interest in designing a methodology to obtain the S_{PT}-N curve and/or the fatigue limit of materials using the SPT is evident, especially when the amount of material available is scarce. To achieve this, it is necessary not only to establish an optimal testing methodology, in which the loads do not exceed those for obtaining yield load (P_y), but also to evaluate possible correlations between fatigue parameters obtained through SPT and those from standard tests. For instance, for fatigue limit, a straightforward way to establish such correlations is to use correction factors, k_i, that modify the value of the fatigue limit obtained under standard conditions, S_f, to account for all factors that influence this limit under different conditions, such as the SPT-fatigue test, S_{f_SPT}, Eq. (3) [36,37].

$$S_{f\_SPT} = k_a k_b k_c k_d k_e k_f \cdot S_f \quad (3)$$

Each of these factors takes into account the influence of all variables affecting fatigue behavior, such as the specimen's surface finish (k_a), its size (k_b), stress distribution in the test (k_c), temperature (k_d), uncertainty (k_e), or the presence of stress concentrators (k_f), [36,37]. The effect of mean stress and the potential presence of residual stresses on the specimens must also be taken into account.

Therefore, the objective of this work is to assess the use of SPT in the fatigue characterization of structural steels, developing a methodology to obtain the S_{PT}-N curves and the fatigue limit S_{f_SPT}. By comparing these parameters with those of standard rotating beam fatigue tests, correlations were established for structural steel S355. The accuracy of these correlations was evaluated by applying them to a tempered-martensitic structural steel (42CrMo4) which has significantly different fatigue behavior from S355.

2. Materials

For the development of the methodology, a widely used structural steel, S355, common in the wind energy sector [38], was employed. To validate the results, a 42CrMo4 steel proposed as an ideal candidate for low-pressure hydrogen storage vessels was also used. Fig. 2 shows the microstructure of the two materials: a mixture of ferrite (black phase) and pearlite (white phase) for S355 (Fig. 2.a) and tempered martensite for 42CrMo4 (Fig. 2.b).

The tensile mechanical properties of the steels were obtained both through tensile tests and SPT. Tensile tests were doing according to the UNE-EN ISO 6892 [39] using standard round specimens with a diameter of 10 mm. For the SPT, square specimens (10x10x0.5 mm) and a testing device (punch diameter of 2.5 mm and lower die hole diameter of 4 mm) were used [24]. The punch displacement was measured using a COD extensometer. All the tests were carried out at a constant displacement rate of 0.2 mm/min, employing lubrication to avoid frictional effects. Al least three specimens were used for each type of test.

The values of the yield strength, σ_{ys}, ultimate tensile strength, σ_{ut}, and elongation, e, of the steels obtained from the two tests are summarized in Table 1. The correlations proposed by T.E. García et al [11] were used to extract the tensile parameters with the SPT (α = 0.346, β = 0.277). The value of P_y, also included in Table 1, was obtained using the t/10 method described in that work [11]. As can be seen in Table 1, the strength parameters (σ_{ys} and σ_{ut}) obtained by the two methods are quite similar.

Based on these results, the average value of the SPT yield load, P_y (261 N ± 13 for S355 steel and 417 N ± 33 for 42CrMo4 steel), will be used as a reference for establishing maximum loads in the SPT-fatigue tests.

3. Fatigue behavior under rotating beam fatigue tests

The rotating beam fatigue tests of S355 steel were conducted on specimens with a circular section as stipulated in [4,41], with a

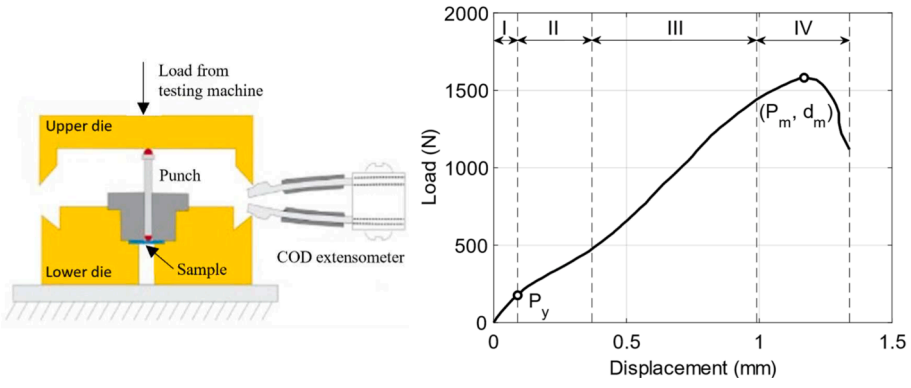

Fig. 1. SPT test: a) General configuration [11]; b) Load-displacement SPT curve.

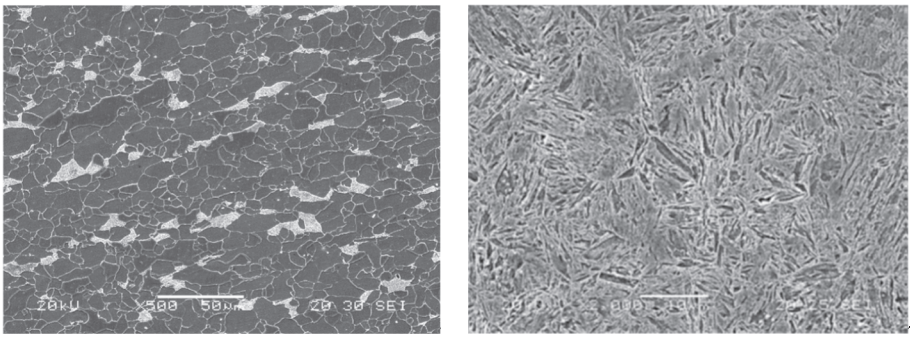

a) b)

Fig. 2. Microstructures of a) S355 steel and b) 42CrMo4 steel.

Table 1
Tensile properties of S355 steel [15] and 42CrMo4 steel [40].

	SPT		Tensile		
	P_y (N)	σ_{ys_SPT} (MPa)	σ_{ys} (MPa)	σ_{ut} (MPa)	e (%)
S355	261 ± 13	361 ± 9	386 ± 4	472 ± 3	32 ± 0.1
42CrMo4	417 ± 33	577 ± 46	622 ± 2	710 ± 5	23 ± 0.6

calibrated zone diameter of 4 ± 0.02 mm, as shown in Fig. 3. After machining, the specimens were ground and polished, ensuring a surface roughness, R_a, of less than 0.2 μm in accordance with ISO EN 1143 [4].

The tests were conducted at room temperature using a "Microtest EFFR4P-100", specifically designed for testing small specimens. The specimen temperature during the test was continuously monitored with the assistance of a pyrometer integrated into the testing machine. The specimens were tested with alternating stress values, S_a, always below the yield strength of the steel, using a frequency of 30 Hz. The goal was merely to obtain a general reference for the behavior of this steel during rotating beam fatigue tests to compare it with the results obtained from the SPT-fatigue test.

To determine the S-N curve, at least two specimens were tested at the same stress level, and the number of cycles required to cause specimen failure was recorded. The Gerber procedure was used to determinate the fatigue limit. Specimens which suffered no damage after 10 million cycles were considered run-out and the next specimen was subjected to a stress level 10 % higher. In case of failure, the next specimen was subjected to a stress level 5 % lower [42].

Fig. 4 presents the results along with the potential Basquin-type fit (Eq. (4)) resulting in the S-N curve for this steel. The coefficients

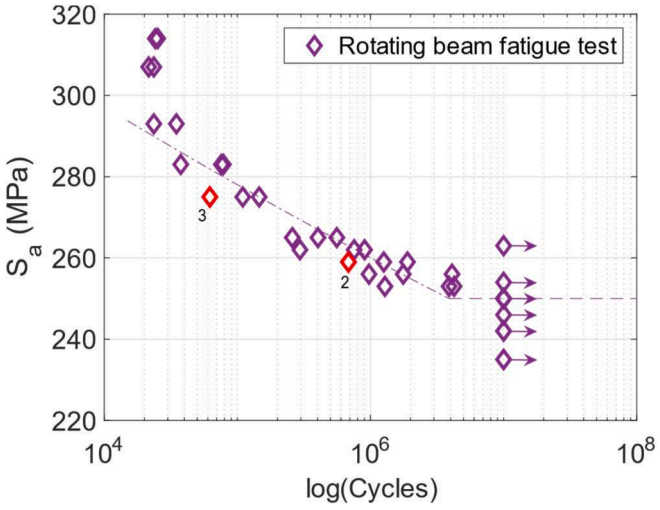

Fig. 4. S-N curve of S355 steel under rotating beam fatigue test.

obtained were σ'_f = 389 MPa and b = − 0.029. The fatigue limit obtained, S_f = 250 MPa, is approximately 65 % of the yield stress (50 % of the tensile strength) of the steel. This result is consistent with the general relationship between the rotating beam fatigue limit and tensile strength [43,44], where the fatigue limit is 50 % of the tensile strength (for steels with a tensile strength below 1400 MPa).

$$S_a = \sigma'_f (2N)^b \tag{4}$$

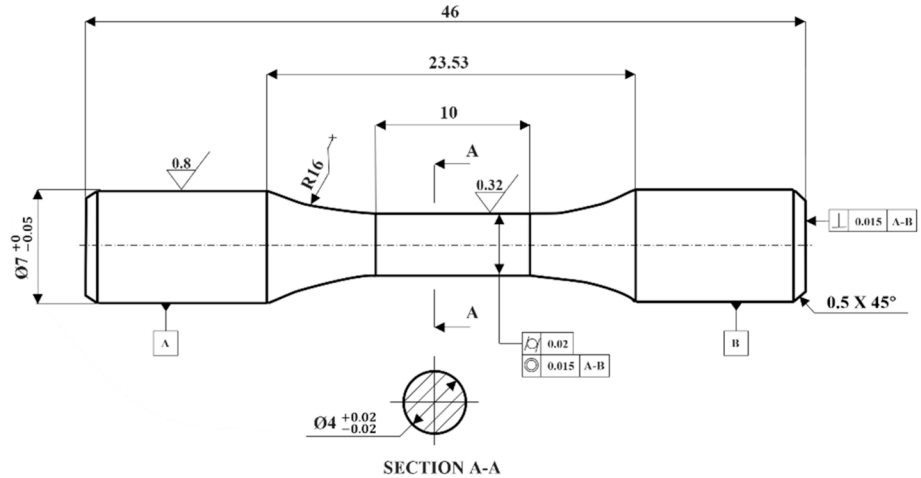

Fig. 3. Geometry of the rotating beam fatigue specimen.

After testing, the fracture surfaces of the specimens were evaluated through scanning electron microscope (SEM). The fatigue damage always started on the surface, sometimes localized (specimen 2, Fig. 5.a), and other times initiating at various points, coalescing as they extended towards the centre of the specimen (specimen 3, Fig. 5.b). The position of both specimens in the S-N curve is highlighted in Fig. 4.

For the 42CrMo4 steel, only the rotating beam fatigue limit, S_f, was needed to compare with that of the SPT fatigue test. Based on the result obtained above, the S_f for this steel was assumed to be 65 % of the yield strength of the material.

4. Analysis of fatigue behavior with SPT

4.1. Development of the proposed methodology

The specimens used in these tests had SPT geometry (10x10x0.5 mm) [24], but their surfaces were prepared to meet the maximum roughness requirements specified by fatigue standards ($R_a < 0.2$ μm) to be similar to rotating beam fatigue tests.

The same device used in static SPT was employed for the tests, but it was coupled to a dynamic "Bionix Servohydraulic Test System" equipped with a 15kN load cell. A video camera was added at the bottom of the SPT device to visualize the surface of the specimen under tension throughout the test (Fig. 6). The tests were conducted at room temperature using a frequency of 10 Hz and a load ratio $R = 0.1$.

To determine the S_{PT}-N curve, each specimen was subjected to a maximum load, P_{max}, lower than the P_y value obtained from the static test, so as not to exceed the stress corresponding to the yield stress of the material. Simultaneously, the compliance, C_i, was recorded during the test. As indicated in Eq. (5), C_i is defined as the ratio between the punch displacement, $\Delta d_i = d_{max} - d_{min}$, and the applied load, $\Delta P = P_{max} - P_{min}$, in each cycle. Since the load range, ΔP, remains constant in each test, the presence of damage produces an increase in displacement and, therefore, an increase in compliance.

$$C_i = \frac{\Delta d_i}{\Delta P} \tag{5}$$

Starting from a P_{max} value equal to 90 % of P_y in the first test, the maximum load was successively reduced in the following test until no damage was observed in the tested specimen after 5 million cycles. To detect the presence of damage, compliance was recorded, and the specimen was also monitored by video camera throughout the test. In addition, once the test was stopped and the specimen was removed from the machine, a detailed analysis was conducted using a scanning electron microscope (SEM) to confirm the presence or absence of damage. Finally, if a crack was present, its length was measured.

It should be noted that none of the tested specimens suffered a sudden break that would indicate failure and the conclusion of the SPT-fatigue test. Therefore, it was necessary to establish a criterion for concluding the tests. Thus, if no damage was detected the tests were stopped once 5 million cycles were exceeded. However, if damage was observed, the tests were stopped at different crack lengths to obtain more information about the damage process and its correlation with the variation in compliance.

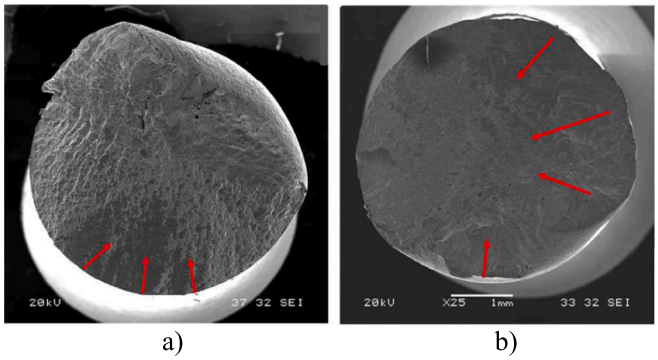

Fig. 5. Fracture surfaces after rotating beam fatigue test (red arrows indicate initiation and growth direction of the damage): a) Specimen 2 and b) Specimen 3.

The staircase procedure was used to determinate the fatigue limit. After testing, the specimens were inspected for any signs of damage using a scanning electron microscope (SEM). If damage was found, the next specimen was subjected to a load level 5 % lower, and the process continued until a load value that caused no damage was identified. Then a load level 10 % higher was applied until damage was observed again. At this point, the search for the fatigue limit was refined by reducing the load in smaller steps until, once again, a load that caused no damage was identified. This final value was taken as the fatigue limit of the material under SPT-fatigue loading, S_{f_SPT}.

Table 2 presents the values of the applied maximum load, $P_{max} = \%P_y$ (ordered from the highest to the lowest percentage of P_y), maximum stress, S_{max}, and the number of cycles at which the test was stopped, N_{stop_cycles}. Table 2 also informs if fatigue damage was observed during the test and the final maximum crack length, a_f (Fig. 6).

Values of stress were calculated applying expression (1) with α = 0.346 according to [11]. As can also be seen in Table 2, some specimens (35 to 38) were tested at load values higher than P_y in order to know their behaviour at such high loads.

To examine the progression of the fatigue damage, Fig. 7.a) shows the compliance variation during the testing of several specimens. Specimen 34 (black dotted curve) was subjected to a $P_{max} = 40\ \%P_y$ and no failure damage was observed after 5 million cycles. As can be seen, after a short initial period (where settlement and equipment adaptation occur), the compliance remains constant until the end of the test.

When the applied load increases, i.e. specimens 1, 2, 16, 21 in Fig. 7.a), the initial settling period can also be seen, but after that, the compliance always grows: faster at the beginning and slower at the end. The inspection of the surfaces of these specimens after the SPT-fatigue test (Fig. 8) indicates fatigue damage. The extent of the crack depends on when the test was stopped.

Specimen 1 (blue dots) was the first to be tested and was stopped at one million cycles. In this test, the compliance grows linearly and quickly at the beginning, until at a certain point at which the growth rate (slope of the C-N curve) slows down considerably. The inspection of the surface of specimen 1 after the test (Fig. 8.a) indicates star-shaped damage, the tips of which almost reach the clamped contour of the specimen. Based on this observation, specimen 2 (red dots in Fig. 7) was subjected to the same load as specimen 1 (90 $\%P_y$), but the test was stopped just at the transition region where the compliance growth rate experimented the change. As can be seen in Fig. 8.b), at that moment, damage was already present on specimen 2, although it was smaller (a_f = 2.01 mm) than that observed in the previous test.

The same behaviour was observed when the applied stress was even lower, but fatigue damage appears, as specimens 16 and 21 in Fig. 7. A closer examination of their compliance variation at a lower number of cycles (Fig. 7.b) reveals that after the settlement period, if damage appears, the compliance value starts to grow and this value increases as the crack length increases. Thus, specimen 16 stopped for a higher compliance value with a crack length of 1.38 mm (Fig. 8.c) while specimen 21 stopped earlier with a crack length of 0.56 mm (Fig. 8.d).

The good agreement between compliance and fatigue damage was also observed in the rest of the specimens. After the settlement period, compliance started to grow, and its value increased as the crack length increased. As the crack grew, it moved away from the point of maximum stress (centre of the specimen) and its growth rate progressively decreased until it stopped as it approached the clamped contour of the specimen.

Based on this extensive experimental campaign it can be stated that compliance is a very good parameter to estimate both the onset of the

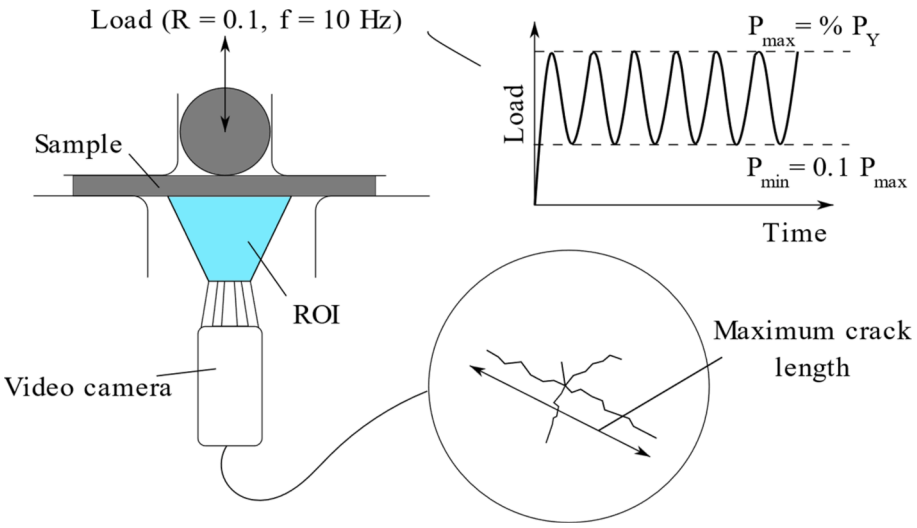

Fig. 6. Setup of SPT-fatigue tests.

Table 2
Results obtained from SPT-fatigue tests of S355 steel.

$\%P_y$	ID	S_{max} (MPa)	N_{stop_cycles}	Damage	a_f (mm)
90	1	325	1,000,000	Yes	3.46
90	2	325	75,435	Yes	2.01
90	3	325	74,781	Yes	1.98
90	4	325	30,000	Yes	1.02
90	5	325	10,435	No	–
90	6	325	5000	No	–
85	7	307	35,000	Yes	0.99
85	8	307	30,000	Yes	0.86
80	9	289	127,470	Yes	2.03
80	10	289	66,957	Yes	1.88
80	11	289	40,000	Yes	0.99
75	12	271	1,250,000	Yes	3.84
75	13	271	28,500	No	–
70	14	253	311,601	Yes	1.16
70	15	253	200,000	Yes	2.34
70	16	253	179,009	Yes	1.38
70	17	253	150,000	Yes	1.24
70	18	253	133,841	Yes	1.05
70	19	253	100,011	Yes	0.79
70	20	253	64,979	Yes	0.87
70	21	253	58,306	Yes	0.56
70	22	253	50,958	Yes	0.83
65	23	235	150,000	Yes	0.64
65	24	235	4757	No	–
60	25	217	286,637	Yes	0.5
50	26	181	5,000,000	Yes	4.5
50	27	181	4,190,144	Yes	4.28
50	28	181	1,572,720	Yes	4.4
50	29	181	912,310	Yes	2.63
45	30	162	5,000,000	Yes	3.8
45	31	162	2,241,794	Yes	2.27
45	32	162	1,778,020	Yes	1.32
40	33	144	5,000,000	No	–
40	34	144	5,000,000	No	–
120	35	433	120,694	Yes	3.78
105	36	379	46,482	Yes	1.73
100	37	361	281,290	Yes	3.85
100	38	361	34,463	Yes	1.68

damage and its extent in SPT-fatigue tests.

4.2. S_{PT}-N curves

Fig. 9 shows the values of maximum applied stress vs number of cycles at the end of the test for all specimens. It is important to note that in the SPT-fatigue test, the number of cycles at the end of the test does not necessarily indicate that damage has been detected; it simply reflects the point at which the test was stopped. In some cases, there may be significant damage to the material, while in others, no damage was observed. The colour of the stars indicates the size of the damage suffered by the end of the test: no damage in red, less than 1 mm in black, between 1 and 3 mm in pink, and between 3.5 and 4.5 mm in blue.

Fig. 9 also shows the S-N curves corresponding to different compliance increments: $\Delta C = 0$ mm/N (no damage), $\Delta C = 2{\cdot}10^{-5}$ mm/N, $\Delta C = 2{\cdot}10^{-4}$ mm/N and $\Delta C = 4.5{\cdot}10^{-4}$ mm/N. The fatigue limit of the material $S_{f\_SPT} = 0.4{\cdot}\sigma_{ys\_SPT} = 144$ MPa, is also represented in Fig. 9.

As can be seen, all the specimens that exhibited no damage (red stars) are located to the left of the S-N curve corresponding to $\Delta C = 0$ mm/N. The specimens that showed damage smaller than 1 mm (black stars) are located around the S-N curve of $\Delta C = 2{\cdot}10^{-5}$ mm/N. Those with damage sizes between 1 and 3 mm (pink stars) are distributed around the S-N curves of $\Delta C = 2{\cdot}10^{-4}$ mm/N and $\Delta C = 4.5{\cdot}10^{-4}$ mm/N. Finally, specimens with damage sizes longer than 3.5 mm are located on the right, far from the last S-N curve.

These observations indicate that S-N curves based on different compliance variations are associated with different levels of damage and could therefore be used as *iso*-damage curves (*iso*-ΔC curves).

Some tests were conducted with load values higher than P_y. As higher stresses were applied beyond the material's yield stress, the damage already exhibits significant plastic deformation, as shown in Fig. 10.a). Due to the large deformation shown in these specimens, fracture micromechanisms could be observed with clarity (Fig. 10.b), where the micromechanism displays the characteristic striations produced by damage growing cycle by cycle.

5. Discussion of results

After analysing the behaviour of S355 steel under two types of fatigue tests, the effect of using one or the other test on the performance of structural steel S355 is assessed by comparing the corresponding S-N curves and their fatigue limits.

5.1. S-N curves obtained by the two methods

Fig. 11 shows the points obtained using the rotating beam fatigue method (diamonds) along with the iso-Δc curves from SPT-fatigue tests. The points indicating failure in rotating beam fatigue tests (represented by diamonds) fall in the zone where damage was also detected in SPT-fatigue tests. This suggests that the results obtained by the two types of tests could be compared. Furthermore, since the rotating beam fatigue

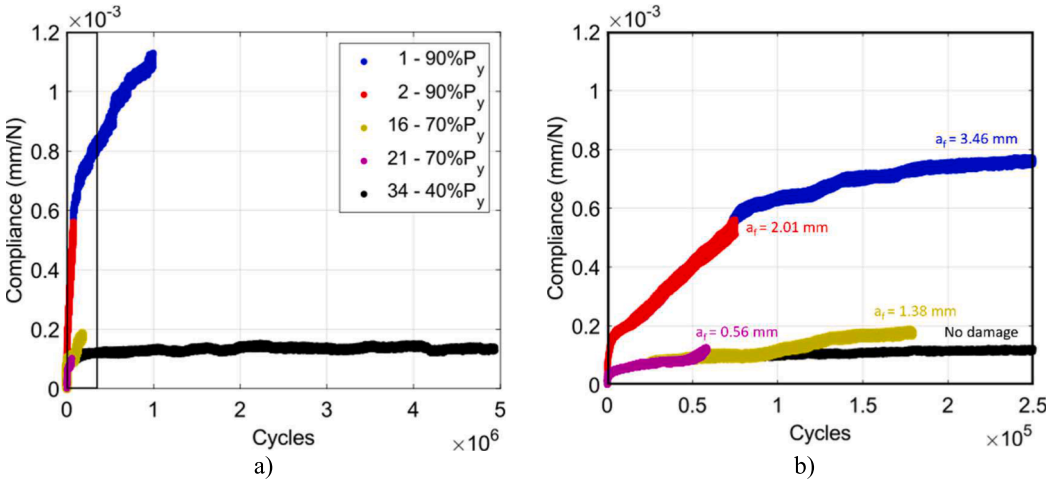

Fig. 7. Compliance variation of the specimens during the SPT-fatigue tests, a) Specimens 1, 2, 10 and 38; b) Enlargement of Fig. 6.a) on the initial zone.

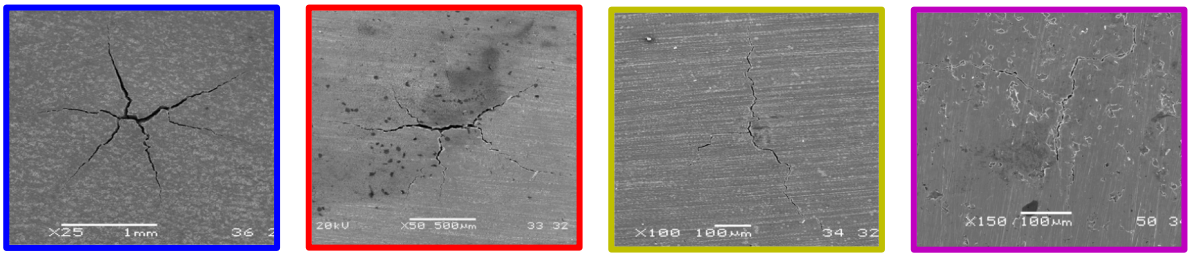

Fig. 8. SEM images of the fracture surface: a) Specimen 1, b) Specimen 2, c) Specimen 16 and d) Specimen 21.

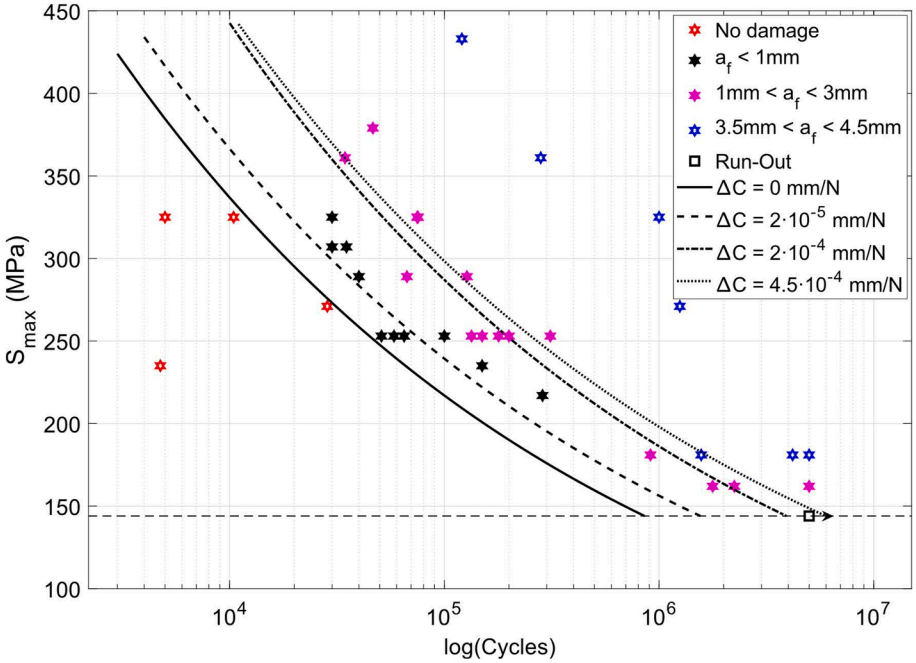

Fig. 9. S_{PT}-N curves obtained in SPT-fatigue tests of S355 steel for different increments of compliance.

S-N curve lies between the S_{PT}-N curves corresponding to compliance increments close to $2{\cdot}10^{-5}$ mm/N, a failure criterion in SPT can be established at the point where a compliance increment of $2{\cdot}10^{-5}$ mm/N is reached, ensuring a safety margin.

5.2. Relationship between fatigue limits

The value obtained for the fatigue limit in the SPT-fatigue test, $S_{f\_SPT} \cong 0.4{\cdot}\sigma_{ys\_SPT} = 144$ MPa, is lower than that obtained in rotating beam

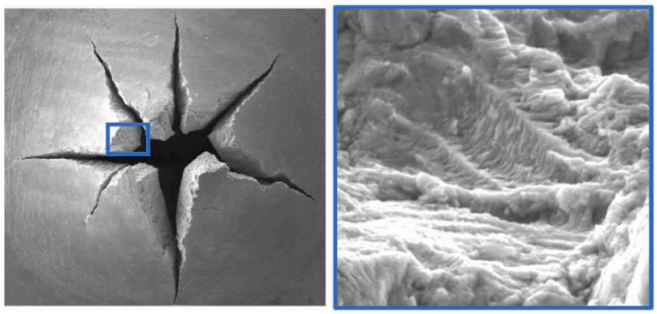

a) b)

Fig. 10. Specimen 35 (P_{max} = 120 % P_y): a) Surface of specimen; b) Typical fatigue damage striations.

fatigue tests, $S_f = 0.65 \cdot \sigma_{ys} = 250$ MPa. This difference is due to the use of different testing methodologies with different values of variables influencing fatigue.

The first effect to consider is the mean stress, which is zero in rotating beam fatigue tests but greater than zero in SPT tests ($R = 0.1$). By correcting the fatigue limit of the SPT test to calculate the equivalent for a mean stress of zero, $S^0_{f\_SPT}$, using an appropriate expression such as the one from Gerber (Eq. (6), where σ_m is the applied mean stress) [36], yields a value of $S^0_{f\_SPT} = 147$ MPa.

$$S^0_{f\_SPT} = \frac{S_{f\_SPT}}{1 - \left(\frac{\sigma_m}{\sigma_{ut}}\right)^2} \tag{6}$$

The remaining difference between the fatigue limits obtained from the two tests can be attributed to the effects of other factors, as expressed in Eq. (3). Due to the characteristics of both tests and the experimental procedure followed, the parameters to consider are the size effect parameter, K_b, and the parameter that accounts for the difference in stress distribution between the two tests, K_c.

Since the surface area of the SPT specimens is smaller than that of rotating beam fatigue tests, the coefficient K_b should be considered greater than 1. Therefore, the key factor making the fatigue limit in SPT-fatigue tests lower than that of rotating beam fatigue tests is K_c.

To better understand the effect of this parameter, it is necessary to compare the maximum tensile stresses borne by rotating beam fatigue specimens (four-point bending) with the tensile stresses borne by SPT specimens for a specific applied load value. For instance, in rotating beam fatigue tests, when a specific load value (e.g. the corresponding to S_f) is applied, the corresponding stress value is only reached at the surface of the specimen, while the rest of the material bears much lower stresses.

The stress distribution of the SPT is not as straightforward, so the analysis of these stresses must be carried out using numerical models. For this purpose, a 2D finite element model was used. This model analyses the stress distribution in the specimen section for different values of load applied by the punch. A complete description of the model can be found in a previous work [45].

In Fig. 12.a), the load–displacement curve of the SPT obtained from the numerical model of S355 steel is presented. In this representation, the experimentally calculated P_y value for the steel is marked with a red point, the load value corresponding to the fatigue limit, $P = 0.4 \cdot P_y$ is marked with a blue point, and the green point represents, as will be seen later, the load level for which no point on the specimen exceeds a stress beyond the yield stress.

Given that the fatigue limit was obtained at applied loads lower than P_y, numerical simulations were performed applying these load values and analysing the stress values attached at different points of the SPT specimen. Fig. 12.b), c) and d) show the stress distribution in the cross-section of the SPT specimen when the applied load is equal to P_y (Fig. 12.b), $0.4 \cdot P_y$ (Fig. 12.c) and $0.21 \cdot P_y$ (Fig. 12.d). Due to the biaxial nature of the stress distribution, only the S_{11} component (radial direction) is represented on half of the specimen.

As seen in Fig. 12.b), when the applied load is equal to P_y, the stresses sustained by a considerable volume of the specimen have already exceeded the yield stress of the steel (386 MPa). Even when the applied load corresponds to the fatigue limit ($0.4 \cdot P_y$, Fig. 12.c), there is a certain volume of the specimen where the stresses slightly exceed the yield stress of the material.

In fact, it is not until a load value equal to 21 % of P_y (Fig. 12.d) that stresses exceeding the yield stress of the material are reached at any

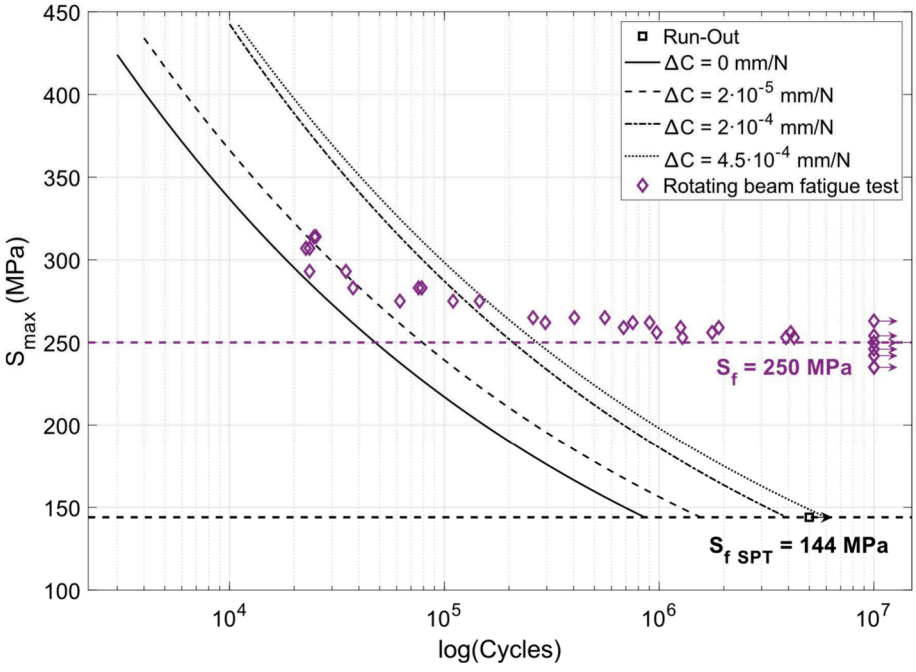

Fig. 11. S-N curve of rotating beam fatigue tests and SPT-fatigue tests for S355 steel.

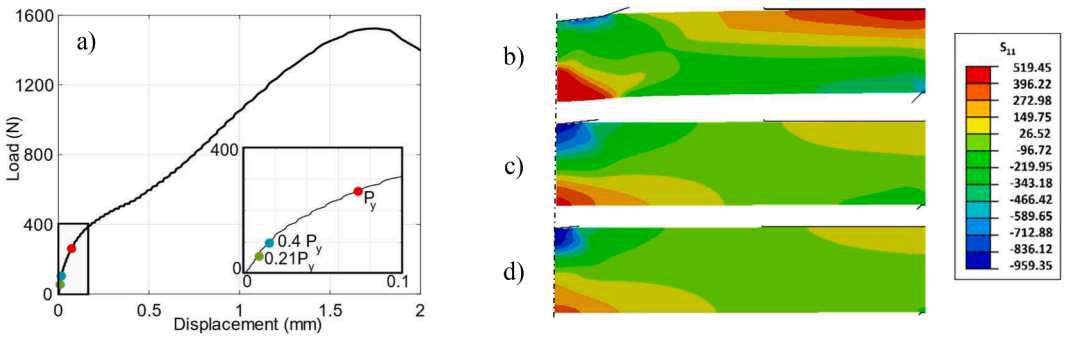

Fig. 12. Numerical analysis of the SPT applied to S355 steel: a) Load-displacement curve; b), c) and d) Stress distributions in half of the specimen at load P_y, $0.4{\cdot}P_y$ and $0.21{\cdot}P_y$ respectively.

point in the specimen.

In light of all the above, it can be stated that the main reason for the differences between the fatigue limits obtained in the rotating beam fatigue tests and in the SPT-fatigue tests is the large difference in the stress distribution in the two tests. In the rotating beam fatigue test the maximum stress reached never exceeds the yield stress of the material and only does so at points on the surface of the specimen. However, in SPT-fatigue tests there is always a considerable volume of the specimen supporting stresses higher than the yield stress.

The effect of both specimen size and the kind of fatigue test must be considered. For this purpose, a coefficient, k_{SPT}, which takes into account the combined effect of these two variables, will be defined. Thus, as long as the specimens used are of the same size as those used in this study and the SPT device is standard (hemispherical punch of 2.5 mm and lower die hole of 4 mm), the combined effect of specimen size and stress distribution can be considered as a single coefficient, k_{SPT}. When using the rotating beam fatigue limit as a reference, k_{SPT} will have a value of 0.587, as shown in Eq. (7):

$$k_{SPT} = k_b k_c = \frac{S^0_{f\_SPT}}{S_f} = 0.587 \tag{7}$$

To corroborate this result, SPT specimens of the 42CrMo4 steel were tested in SPT-fatigue to determine its SPT-fatigue limit. Since it was seen earlier that the fatigue limit of structural steels can be estimated as 65 % of the yield strength of the material, the fatigue limit of this steel is $S_f =$ 404 MPa.

SPT-fatigue tests were conducted using the same procedure as for S355 steel described above. Fig. 13 shows the obtained results. Also, for this steel, the obtained fatigue limit corresponds to a stress of approximately 40 % of σ_{ys_SPT}, i.e. $S_{f_{SPT}} = 231$ MPa. So, correcting the effect of non-zero mean stress $S^0_{f\_SPT} = 236$ MPa a $k_{SPT} = 0.584$ (similar to that obtained for S355 steel, Eq. (7)) was obtained. This result confirms the validity of the proposed coefficient, k_{SPT}, for estimating the fatigue limit of the rotating beam test through that obtained from SPT-fatigue tests.

6. Conclusions

In this work, the fatigue behaviour of two structural steels has been analysed using the Small Punch test. After an extensive experimental work that also included the fatigue characterisation of one of them by rotating beam fatigue tests, the main conclusions obtained are the following:

1. Using rotating beam fatigue tests, the S355 steel showed a stress-life curve that fits a Basquin law with parameters $\sigma'_f = 389$ MPa and b = − 0.029, and a fatigue limit of 65 % of the steel yield stress.

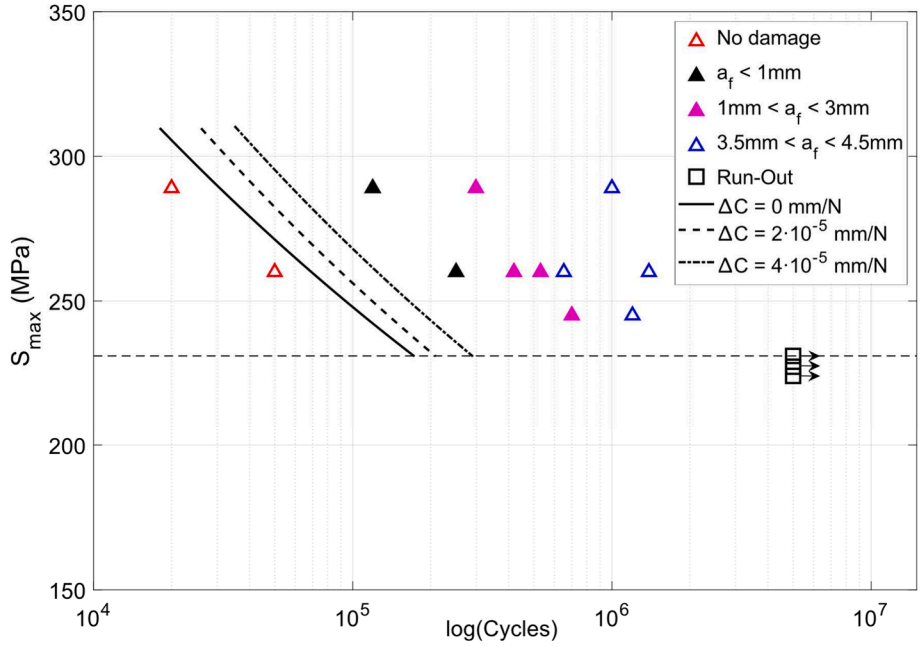

Fig. 13. S_{PT}-N curves obtained in SPT-fatigue tests of 42CrMo4 steel for different increments of compliance.

2. To use the SPT as a fatigue test, an experimental methodology based on the specimen compliance variation has been developed.
3. Based on that methodology, different S_{PT}-N (*iso*-damage) curves of the S355 steel have been defined. The SPT-fatigue limit, with a value of 40 % of the steel yield stress, was also obtained.
4. In SPT-fatigue tests, damage always initiates in the central region of the specimen at the face opposite to the punch contact, subsequently branching out into a star-like pattern with tips growing towards the specimen contour and stopping when they near the clamped region.
5. A correlation coefficient, k_{SPT}, has been proposed to relate the rotating beam fatigue limit (S_f) and the SPT fatigue limit ($S_{f,SPT}$). The k_{SPT} coefficient takes into account the combined influence of the different specimen sizes and stress distributions.
6. The validity of k_{SPT} coefficient has been confirmed comparing the fatigue limits from the two kinds of tests applied to a 42CrMo4 steel.
7. This work opens the door to the application of the SPT in the fatigue characterization of structural steels.

CRediT authorship contribution statement

S. Otero: Writing – review & editing, Writing – original draft, Software, Methodology, Investigation, Formal analysis, Data curation. **G. Álvarez:** Writing – review & editing, Software, Methodology, Formal analysis, Data curation, Conceptualization. **M.M. Llera:** Software, Data curation. **C. Rodríguez:** Writing – review & editing, Validation, Resources, Project administration, Methodology, Investigation, Data curation, Conceptualization.

Declaration of competing interest

The authors declare that they have no known competing financial interests or personal relationships that could have appeared to influence the work reported in this paper.

Acknowledgements

S. Otero thanks the Spanish Ministry of Universities for the FPI Predoctoral Fellowship (PID2021-124768OB-C22 (PRE2022-103206)) and the Principality of Asturias for the funding received through grants AYUD-2021-57532. Our thanks also to the Scientific and Technical Service, University of Oviedo, for the use of the SEM JEOL-JSM5600 scanning electron microscope.

Data availability

The data that has been used is confidential.

References

[1] Zaidi R, Sedmak A, Kirin S, Grbovic A, Li W, Lazic Vulicevic L, et al. Risk assessment of oil drilling rig welded pipe based on structural integrity and life estimation. Eng Fail Anal 2020;112. https://doi.org/10.1016/j.engfailanal.2020.104508.
[2] X. Sun, J. Yao, G. Chai, Y. Bao, Thickness effects of base wall and inlet pipe on the structural integrity of reactor pressure vessels considering ductile-to-brittle transition, Eng Fail Anal 105 (2019) 1032–1044, https://doi.org/10.1016/j.engfailanal.2019.05.036.
[3] ASTM E466-21 Standard Practice for Conducting Force Controlled Constant Amplitude Axial Fatigue Tests of Metallic Materials.
[4] Iso, 1143:2021: Rotating bar bending fatigue testing. ISO, International. (2010).
[5] J.M. Meza, C.A. Chaves, J.M. Vélez, Indentation Techniques: Mechanical Properties Measurement of Ceramics 73 (2006) 81–93.
[6] A. Gouldstone, N. Chollacoop, M. Dao, J. Li, A.M. Minor, Y.L. Shen, Indentation across size scales and disciplines: Recent developments in experimentation and modeling, Acta Mater 55 (2007) 4015–4039, https://doi.org/10.1016/j.actamat.2006.08.044.
[7] S. Pahlavanyali, A. Rayment, B. Roebuck, G. Drew, C.M.F. Rae, Thermo-mechanical fatigue testing of superalloys using miniature specimens, Int J Fatigue 30 (2008) 397–403, https://doi.org/10.1016/j.ijfatigue.2007.01.051.
[8] T.D. Shikalgar, B.K. Dutta, J. Chattopadhyay, Assessment of fracture resistance data using p-SPT specimens, Theoretical and Applied Fracture Mechanics 98 (2018) 167–177, https://doi.org/10.1016/j.tafmec.2018.10.003.
[9] R. Procházka, J. Džugan, Low cycle fatigue properties assessment for rotor steels with the use of miniaturized specimens, Int J Fatigue 154 (2022), https://doi.org/10.1016/j.ijfatigue.2021.106555.
[10] C. Rodríguez, J. García Cabezas, E. Cárdenas, F.J. Belzunce, C. Betegón, Mechanical Properties Characterization of Heat-Affected Zone Using the Small Punch Test, Welding Rereach. (2009).
[11] T.E. García, C. Rodríguez, F.J. Belzunce, C. Suárez, Estimation of the mechanical properties of metallic materials by means of the small punch test, J Alloys Compd 582 (2014) 708–717, https://doi.org/10.1016/j.jallcom.2013.08.009.
[12] E. Altstadt, H.E. Ge, V. Kuksenko, M. Serrano, M. Houska, M. Lasan, et al., Critical evaluation of the small punch test as a screening procedure for mechanical properties, Journal of Nuclear Materials 472 (2016) 186–195, https://doi.org/10.1016/j.jnucmat.2015.07.029.
[13] M. Bruchhausen, S. Holmström, I. Simonovski, T. Austin, J.M. Lapetite, S. Ripplinger, et al., Recent developments in small punch testing: Tensile properties and DBTT, Theoretical and Applied Fracture Mechanics 86 (2016) 2–10, https://doi.org/10.1016/j.tafmec.2016.09.012.
[14] J. Calaf-Chica, P.M. Bravo Díez, M. Preciado Calzada, D. Ballorca-Juez, A systematic FEM analysis of the influence of mechanical properties in the reliability of the correlation methods in the small punch test, Int J Mech Sci 153–154 (2019) 299–309, https://doi.org/10.1016/j.ijmecsci.2019.02.013.
[15] Álvarez G, Rodríguez C, Belzunce FJ, García TE. Use of notched small punch test specimens for the determination of fracture properties in structural steels. Theoretical and Applied Fracture Mechanics 2020;106. https://doi.org/10.1016/j.tafmec.2019.102442.
[16] Manahan MP, Argon AS, Harling OK. The development of a miniaturized disk bend test for the determination of postirradiation mechanical properties. 1981.
[17] S. Kim, U. Ro, T. Lee, M.K. Kim, Evaluation of creep properties considering the friction effect of the small punch test, Eng Fract Mech 298 (2024), https://doi.org/10.1016/j.engfracmech.2024.109879.
[18] García-Blanco I, García TE, Cabezas JG, González R, Álvarez G, Rodríguez C. Use of the small punch test for mechanical characterization of co– based laser cladding joint. Eng Fail Anal 2024;159. https://doi.org/10.1016/j.engfailanal.2024.108129.
[19] Álvarez G, Zafra A, Rodríguez C, Belzunce FJ, Cuesta II. SPT analysis of hydrogen embrittlement in CrMoV welds. Theoretical and Applied Fracture Mechanics 2020;110. https://doi.org/10.1016/j.tafmec.2020.102813.
[20] R. Lancaster, G. Davies, H. Illsley, S. Jeffs, G. Baxter, Structural Integrity of an Electron Beam Melted Titanium Alloy, Materials. 9 (6) (2016) 470, https://doi.org/10.3390/ma9060470.
[21] X. Jiang, P. Du, M. Li, H.S. Lai, F. Liu, Y. Zhong, et al., Investigating effects of element composition on the microstructure and mechanical properties of three types FeCrAl alloys through small punch test, Mater Des 238 (2024), https://doi.org/10.1016/j.matdes.2024.112712.
[22] Y. Zu, Y. Cao, Y. Zhen, F. Li, G. Wu, Determination on the fracture toughness of the welded joints of X80 pipeline steels based on small punch test, Eng Fract Mech 291 (2023), https://doi.org/10.1016/j.engfracmech.2023.109525.
[23] T. Melkior, D. Terentyev, C.C. Chang, A. Bakaev, S. Holmström, S. Lebediev, et al., Mechanical properties of structural metallic alloys for nuclear applications deduced by small punch test, Journal of Nuclear Materials 583 (2023), https://doi.org/10.1016/j.jnucmat.2023.154521.
[24] UNE-EN 10371:2022; Small punch test method.
[25] ASTM E3205-20: Standard Test Method for Small Punch Testing of Metallic Materials.
[26] Wang X, Xu L, Zhao L, Han Y. Evaluation of defect-related fatigue performance of additive manufacturing GH4169 via small punch test. Theoretical and Applied Fracture Mechanics 2023;128. https://doi.org/10.1016/j.tafmec.2023.104162.
[27] Zhao L, Wang X, Xu L, Han Y, Jing H. Fatigue performance of Hastelloy X at elevated temperature via small punch fatigue test. Theoretical and Applied Fracture Mechanics 2021;116. https://doi.org/10.1016/j.tafmec.2021.103118.
[28] R. Prakash, Study of Fatigue Properties of Materials through Cyclic Automated Ball Indentation and Cyclic Small Punch Test Methods, Key Eng Mater (2017).
[29] D. Holländer, D. Kulawinski, A. Weidner, M. Thiele, H. Biermann, U. Gampe, Small-scale specimen testing for fatigue life assessment of service-exposed industrial gas turbine blades, Int J Fatigue 92 (2016) 262–271, https://doi.org/10.1016/j.ijfatigue.2016.07.014.
[30] M. Li, S. Maskill, Z. Wen, Z. Yue, W. Sun, A miniaturized thin-plate low cycle fatigue test method at elevated temperature, Fatigue Fract Eng Mater Struct 45 (2022) 1361–1378, https://doi.org/10.1111/ffe.13665.
[31] R.V. Prakash, A. Subbiah, Evaluation of Fatigue Data through Miniature Specimen Test Techniques. American Society of Mechanical Engineers, Pressure Vessels and Piping Division (publication) PVP vol. 1A (2015), https://doi.org/10.1115/PVP2015-45339.
[32] Prakash R V., Dhaka P, Prasad Reddy G V., Sandhya R. Understanding the fatigue response of small volume specimens through novel fatigue test methods – Experimental results and numerical simulation. Theoretical and Applied Fracture Mechanics 2019;103. https://doi.org/10.1016/j.tafmec.2019.102304.
[33] R.V. Prakash, S. Arunkumar, Evaluation of Damage in Materials Due to Fatigue Cycling Through Static and Cyclic Small Punch Testing. Small Specimen Test, Techniques 6th Volume (2015) 168–186, https://doi.org/10.1520/STP157620140011.
[34] R.J. Lancaster, S.P. Jeffs, H.W. Illsley, C. Argyrakis, R.C. Hurst, G.J. Baxter, Development of a novel methodology to study fatigue properties using the small

punch test, Materials Science and Engineering: A 748 (2019) 21–29, https://doi.org/10.1016/j.msea.2019.01.074.
[35] D.T.S. Lewis, R.J. Lancaster, S.P. Jeffs, H.W. Illsley, S.J. Davies, G.J. Baxter, Characterising the fatigue performance of additive materials using the small punch test, Materials Science and Engineering: A 754 (2019) 719–727, https://doi.org/10.1016/j.msea.2019.03.115.
[36] Norman E.Dowling. Mechanical Behavior of Materials_Engineering Methods for Deformation, Fracture, and Fatigue. Fourth Edition.
[37] EN 1993-1-9:2013: Eurocode 3: Design of steel structures - Part 1-9: Fatigue.
[38] D. Forni, B. Chiaia, E. Cadoni, High strain rate response of S355 at high temperatures, Mater Des 94 (2016) 467–478, https://doi.org/10.1016/j.matdes.2015.12.160.
[39] UNE-EN ISO 6892-1: 2020. Metallic materials- Tensile testing- Part 1: Method of test at room temperature (ISO 6892-1:2019) 2020.
[40] A. Zafra, L.B. Peral, J. Belzunce, C. Rodríguez, Effect of hydrogen on the tensile properties of 42CrMo4 steel quenched and tempered at different temperatures, Int J Hydrogen Energy 43 (2018) 9068–9082, https://doi.org/10.1016/j.ijhydene.2018.03.158.
[41] ISO 1099:2017 Metallic Materials- Fatigue testing- Axial force- controlled method-ISO International.
[42] Iso 12107:2012., Metallic materials. Fatigue testing. Statistical planning and analysis of data. ISO, International. (2003).
[43] E. Zahavi Fatigue Design: Life Expectancy of Machine Parts (1st ed.). 1996 CRC Press 10.1201/9780203756133.
[44] Atkinson RJ. Designing Against Fatigue.R. B. Heywood. Chapman & Hall, London. 1962. 436 pp. Illustrated.84S. The Journal of the Royal Aeronautical Society. 1963; 67(627):195-195. doi:10.1017/S0368393100078317.
[45] Peñuelas I, Rodríguez C, Belzunce FJ, Betegón C. Analytical and experimental determination of the fracture toughness by means of small punch test specimens notched with a femtolaser. 2017.